


# Effects of boundary conditions on the core-halo mass scaling relation of fuzzy dark matter structures

Iván Álvarez-Rios<sup>\*</sup> and F. S. Guzmán<sup>†</sup>

*Instituto de Física y Matemáticas, Universidad Michoacana de San Nicolás de Hidalgo, Edificio C-3, Cd. Universitaria, 58040 Morelia, Michoacán, México*

 (Received 4 January 2024; revised 10 June 2024; accepted 26 June 2024; published 22 July 2024)

We simulate multicore merger of fuzzy dark matter in a periodic domain until it relaxes and forms the typical core-halo structure, found both in small domain analyses as well as in structure formation simulations. Using a reference potential gauge invariance of the Schrödinger-Poisson system of equations, we use different values of the reference gravitational potential at the boundaries and illustrate how it affects the core-halo scaling relation of the resulting core-halo structure. This result demonstrates that using different boundary conditions for the reference gravitational potential in various simulations may contribute to the diversity of the scaling relation.

DOI: [10.1103/PhysRevD.110.023530](https://doi.org/10.1103/PhysRevD.110.023530)

## I. INTRODUCTION

Ultralight Bosonic dark matter is a candidate currently under study because it shows interesting implications, it behaves like cold dark matter (CDM) at large scales, whereas at local galactic scales it forms clumps with a core-tail structure, because its small mass, of order  $10^{-24}$ – $10^{-20}$  eV/ $c^2$ eV, implies a large de Broglie wavelength that prevents the formation of cuspy density profiles. It is then thought that this property may help reconciling the cusp-core and too big to fail problems of CDM. More properties and restrictions of this dark matter model are well developed in recent reviews [1–5].

The state of the art of the subject involves various aspects, most of them based on the implications from each time more elaborate structure formation simulations (e.g. [6–10]) based on the solution of the Schrödinger-Poisson (SP) system of equations. Probably the most important result of these simulations is that they demonstrate the formation of core-tail structures with a solitonic core surrounded by a high kinetic energy halo that on average can be fitted with the Navarro-Frenk-White profile. A pattern that has called the attention of these structures is that they follow a core-halo mass scaling relation that may contain information about its formation history. The SP system of equations governing the evolution of this dark matter can be expressed as follows:

$$i\hbar\partial_t\Psi = -\frac{\hbar^2}{2m_B}\nabla^2\Psi + m_B V\Psi + g|\Psi|^2\Psi, \quad (1)$$

$$\nabla^2 V = 4\pi G(\rho - \bar{\rho}), \quad (2)$$

where  $\hbar$  and  $G$  are Planck and gravitational constants,  $m_B$  is the boson mass,  $\Psi$  the parameter order of the boson gas,  $V$  the gravitational potential sourced by the density of the boson gas itself given by  $\rho := m_B|\Psi|^2$ ,  $g$  is the self-interaction parameter, which for fuzzy dark matter (FDM) [11] is set to  $g = 0$ , and  $\bar{\rho}$  is the spatial averaged density

$$\bar{\rho} := \frac{1}{|D|} \int_D \rho d^3x, \quad (3)$$

calculated over a given domain  $D$  with volume  $|D|$ . The usual scalar quantities used to monitor the properties of a given evolving structure of FDM are the total mass  $M$ , kinetic energy  $K$ , and gravitational energy  $W$  given by

$$M := \int_D \rho d^3x, \quad (4)$$

$$K := -\frac{\hbar^2}{2m_B} \int_D \Psi^* \nabla^2 \Psi, \quad (5)$$

$$W := \frac{1}{2} \int_D \rho V d^3x. \quad (6)$$

In [6], based on the results from structure formation simulations (SFS) a scaling relation was found between these quantities:

$$M_c = \text{constant} \left( \frac{E}{M} \right)^{1/2}, \quad (7)$$

<sup>\*</sup>Contact author: [ivan.alvarez@umich.mx](mailto:ivan.alvarez@umich.mx)

<sup>†</sup>Contact author: [francisco.s.guzman@umich.mx](mailto:francisco.s.guzman@umich.mx)

where  $M_c$  is the integrated core mass of the also found universal attractor soliton density profile

$$\rho_{\text{core}}(r) = \rho_c \left[ 1 + 0.091 \left( \frac{r}{r_c} \right)^2 \right]^{-8}, \quad (8)$$

characterized by a core radius  $r_c$  and a central density  $\rho_c$ , whose integral is explicitly

$$M_c = 4\pi \int_0^{r_c} \rho_{\text{core}}(r) r^2 dr \approx 2.790 \rho_c r_c^3, \quad (9)$$

and where  $E = K + W$  is the total energy. The scaling relation (7) associates the core mass on the left with the halo dispersion relation on the right. This result was confirmed using a controlled set of multicore merger local simulations that collapse to form core-halo structures [12].

Later on, in [13] a different scaling relation was proposed, in which the core mass is normalized with  $M$ , which leaves a scaling relation invariant under the lambda scaling [14]

$$\begin{aligned} \{t, \vec{x}, \Psi, V, \rho\} &\rightarrow \{\lambda^{-2}t, \lambda^{-1}\vec{x}, \lambda^2\Psi, \lambda^2V, \lambda^4\rho\}, \\ \{M, K, W, E\} &\rightarrow \{\lambda M, \lambda^3K, \lambda^3W, \lambda^3E\}, \end{aligned}$$

of the SP system (1) and (2). The proposed scaling relation reads

$$\frac{M_c}{M} = \beta \Xi^\alpha, \quad \Xi := \frac{|E|}{M^3} \left( \frac{\hbar}{Gm_B} \right)^2, \quad (10)$$

where  $\beta$  is a constant. This relation is obtained from binary mergers, and it was found for a number of simulations with different initial conditions that  $\alpha \sim 1/4$  in the case of mergers in orbit, and  $\alpha \sim 1/6$  for head-on collisions. For multicore mergers similar to those in [12] it was found that  $\alpha$  is between  $1/6$  and  $1/2$ . An important signature of this analysis is that isolation boundary conditions are used for the simulations.

In [7] a similar study based on multisoliton mergers finds that  $\alpha \sim 1/3$ , more precisely bounded between  $1/4$  and  $1/2$ . The difference with the results in [13] may be due to the boundary conditions used, isolated in [13] and periodic in [7], that help preserving energy and mass in the whole domain during the simulations.

Other studies based on different core formation histories find  $\alpha \sim 1/5$ – $1/4$  as a result of the fitting of final core-halos,  $\alpha \sim 1/3$  when the scaling relation is spatially averaged [15]. From spherical collapse it was found that  $\alpha \sim 1/3$  [16,17]. More recently, in [18] the construction of core-halo solutions with spherical symmetry shows  $\alpha \sim 1/3$  whereas when they relax  $\alpha \sim 1/2$ . The differences among the various scaling relations led to the analysis in [19], where the diversity of  $\alpha$  is identified with different

formation histories using a number of different simulations under various physical scenarios [20].

We explore the possibility that this diversity may be due to some implementation details not completely specified in FDM simulations, specifically the boundary conditions for the gravitational potential. In Lagrangian approaches involving for example SPH methods, boundary conditions are not a big problem, because it suffices to change the domain topology by enforcing periodic boundary conditions without imposing reference values to the gravitational potential at any Eulerian boundary. On the other hand, when using Eulerean frame simulations for FDM dynamics, like in the flagship references [7,12,13] among others following a similar approach (e.g. [15,21]), the reference potential seems to be subtle and important.

In order to explain our point, we exploit the  $V_0$ -gauge invariance of the SP system that allows one to set arbitrary potential reference values at the boundaries of the numerical domain. We then produce simulations of multicore-mergers on a periodic domain and study the effect of using different reference gravitational potential on the value of  $\alpha$ .

The paper is organized as follows. In Sec. II we describe the gauge invariance that allows choosing the gravitational potential at boundaries. In Sec. III we study the effects of this gauge invariance on the value of  $\alpha$ , and in Sec. IV we draw some final comments.

## II. THE $V_0$ -GAUGE INVARIANCE

We can distinguish between two scenarios considered in simulations of FDM, one that assumes the system under study remains isolated and boundary conditions implemented at the numerical boundary simulate a transparent surface that allows matter to get off. In this case  $M$  and  $E$  integrated on  $D$ , change in time due to the loss of matter ejected during the gravitational cooling process [22,23], and the quantity  $\Xi$  is not preserved in time. In this case, as done in [13], the boundary conditions are unique, in the sense that the potential at the boundaries is given by  $V = -M/r +$  multipolar terms, where  $r$  is the distance from the domain center to each point of the boundary of the simulation domain  $D$ .

A second scenario corresponds to the use of periodic boundary conditions, that in a way recycle matter and energy components so that the global properties  $M$  and  $E$  are preserved. In this case, the boundary conditions lack of a clear specification, and the value of the gravitational potential at the boundary is not quite specified in various analyses studying the core-halo scaling relation. Between the two types of boundary conditions there are a number of effects that can be only curiosities or have serious implications as discussed in [21], that may depend on the type of boundary condition combined with the domain size of simulations.

The periodic domain is the one we want to focus on, because it is the most used when constructing core-halo

scaling relations in FDM dynamic simulations. We start by pointing out that the SP system is invariant under the  $V_0$ -gauge transformation defined by

$$\{\Psi, V\} \rightarrow \{\Psi e^{-im_B V_0 t/\hbar}, V + V_0\}, \quad (11)$$

that leaves  $\rho$ ,  $M$ , and  $K$  invariant, whereas the gravitational energy suffers the translation

$$W \rightarrow W + V_0 M. \quad (12)$$

Consequently the total energy transforms as  $E \rightarrow E + V_0 M$ , which in turn changes the value of  $\Xi$ . This compromises the scaling relation (10), which is  $V_0$  dependent.

### III. EFFECTS OF $V_0$ ON $\alpha$

#### A. Simulations

We illustrate this effect using a single affordable scenario consisting of the multicore merger that forms a final

core-envelope FDM configuration. Similarly to [7,12,13], we prepare initial data sets with 3–18 solitons, with random masses ranging from  $1.5 \times 10^8 M_\odot$  to  $4 \times 10^8 M_\odot$ , randomly distributed within a cube of side 60 kpc. This cube is centered within the numerical domain, which is a cube of side 80 kpc. We assume the boson mass  $m_B = 10^{-22} \text{ eV}/c^2$ . Initial data are also prepared in such a way that there is no net angular momentum, so that the scaling relation would depend only on  $M$  and  $E$ , and not on the angular momentum like in binary mergers.

We evolve these initial conditions using periodic boundary conditions using the code CAFE-FDM [21,24], that implements a pseudospectral method with the fast Fourier transform to solve the SP system using a discrete form of the Schrödinger equation (1) with the Crank-Nicolson time average. Time and spatial resolutions are  $\Delta = 62.5 \text{ pc}$  and  $\Delta t = 2.5 \times 10^{-3} \text{ Gyr}$  and the evolution lasts 14 Gyr in order to allow the system to relax. We use these simulations to explore the behavior of using different values of  $V_0$ . We define three different boundary values of the gravitational potential:

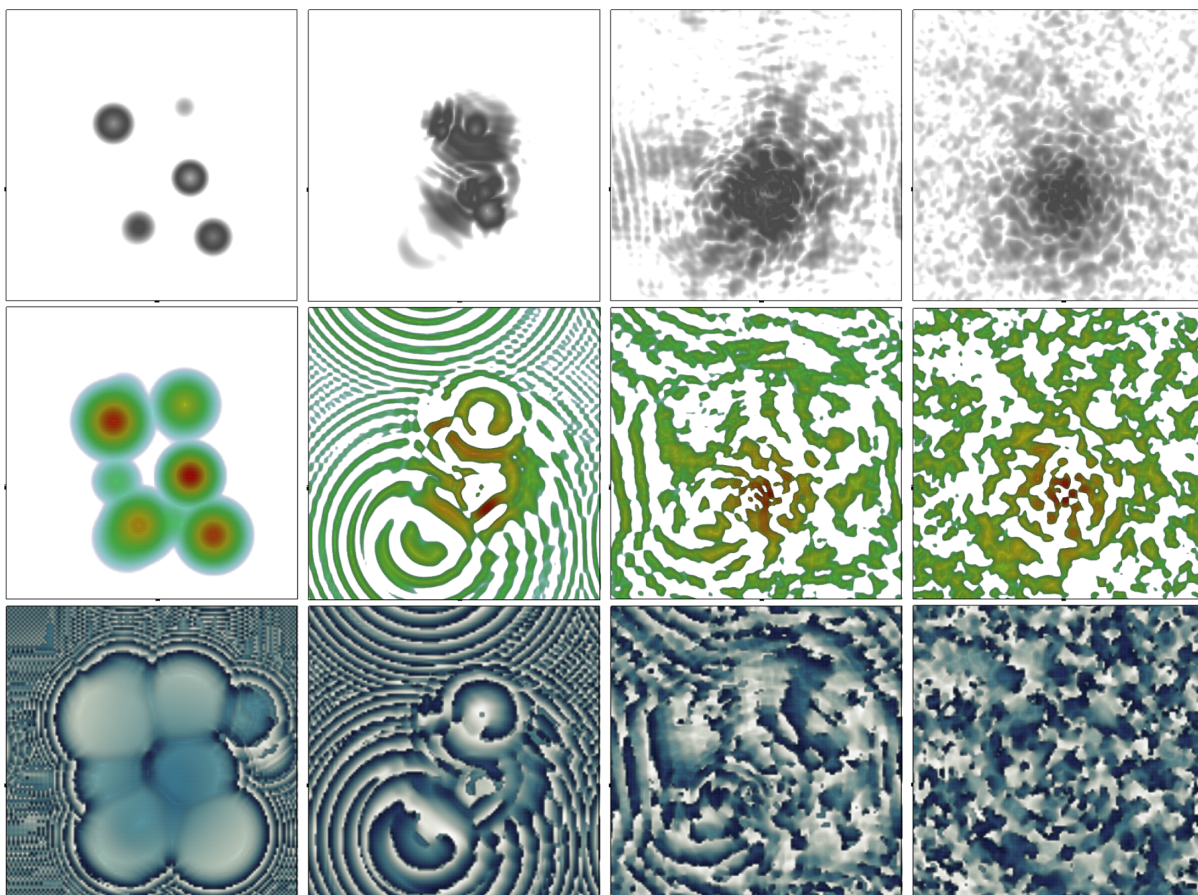


FIG. 1. Snapshots from one of our simulations, for the density  $\rho$  at the top row, the real part of  $\Psi$  at the middle row, and the phase of  $\Psi$  at the bottom. These are taken, from left to right, at times 0, 3, 9, and 14 Gyr, on a plane perpendicular to the  $y$  axis that passes through the final core. The density illustrates the clustering of various initial cores from initial until final time. The real part and phase of  $\Psi$  show the interference patterns and the evolution of the wave function in the periodic domain.



### 1. Potential A

In a first scenario we set the potential at the boundary faces to

$$V_A = V - \max(V) - G \frac{M}{r_{\max}}, \quad (13)$$

where  $\max(V)$  represents the maximum value of  $V$  that happens at the corners of the box, and  $r_{\max} := \sqrt{3} 40$  kpc is half the diagonal length of the cubic domain. This potential is used as an approximation of monopolar boundary conditions used in isolated systems.

### 2. Potential B

We add a constant value  $V_0$  to  $V_A$

$$V_B = V_A + V_0. \quad (14)$$

which corresponds to a simple change of reference of  $V_A$  through the constant  $V_0$  and in principle, according to the invariance (11) would give the same dynamics as with  $V_A$  except for a phase in  $\Psi$ . For this exercise we use two values of the constant  $V_0 = 1843, 3685$  km<sup>2</sup>/s<sup>2</sup>, or equivalently  $V_0 = 5, 10$  in code units.

As an illustration of the evolution of these multicore mergers, in Fig. 1 we show snapshots of the density  $\rho$ ,  $\text{Re}(\Psi)$ , and the phase of  $\Psi$  during the evolution for one of our simulations. The snapshots correspond to 0, 3, 9, and 14 Gyr from left to right, and are taken at a plane perpendicular to the  $y$  axis that passes through the center of the final core. These plots show the process of accumulation of matter during the simulation as well as the behavior of the wave function. We use this time window of evolution in order to have a formed core, whereas for our analysis we calculate space and time averages of the density only during the lapse between 12 and 14 Gyr as detailed below.

### B. Core determination through time-spatial averaging

In order to locate the resulting formed core, we track the maximum density during the evolution lasting 14 Gyr. We then calculate the average density during the last 2 Gyr of simulation over the solid angle as

$$\langle \rho \rangle(r) = \frac{1}{2 \text{ Gyr}} \int_{12 \text{ Gyr}}^{14 \text{ Gyr}} \left[ \frac{1}{4\pi} \int_{\Omega} \rho d\Omega \right] dt. \quad (15)$$

For the simulation of Fig. 1 we illustrate, in gray, the plots of this density at various times within the last 2 Gyr of evolution in the first panel of Fig. 2, corresponding to only the spatial average in formula (15), that is, the expression in square braces. Using this averaged radial density, we fit the parameters  $(\rho_c, r_c)$  of the core using formula (8), which are then

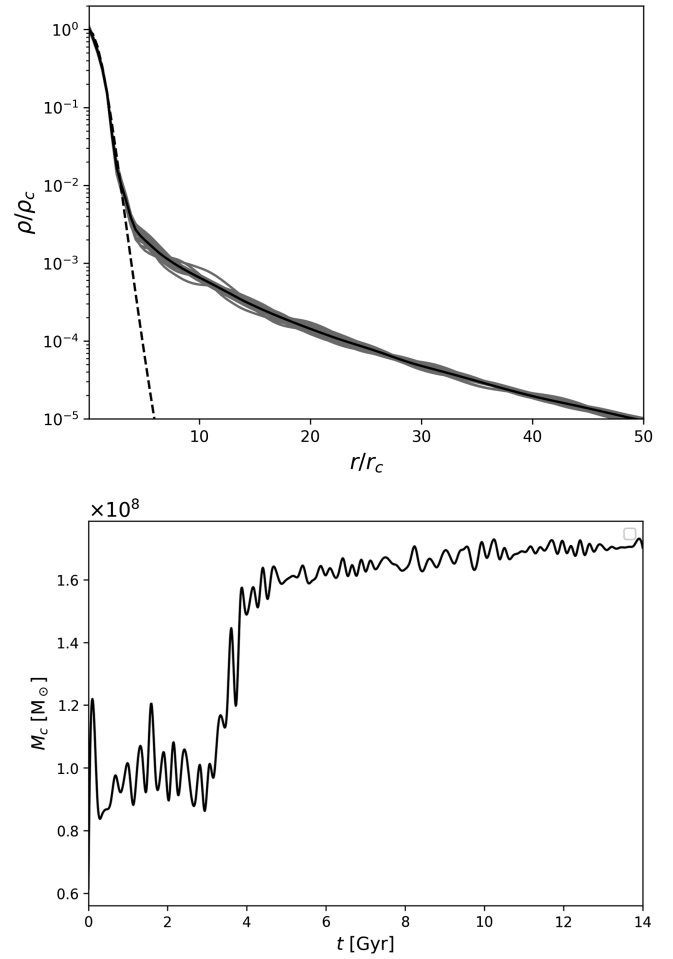


FIG. 2. For the same simulation of Fig. 1 we show various diagnostics. At the top we show in gray, various snapshots of the normalized spatially averaged density between 12 and 14 Gyr and in black the time average of all snapshots, taken every 0.05 Gyr, captured within such time window. Gray lines capture the spatial average of the first integral of formula (15), that is the expression in squared braces, whereas the black line represent the density averaged both, in space and in time using the whole formula (15). The dashed line corresponds to the density profile (8) that better fits the black line. At the bottom we show the core mass  $M_c$  as function of time during the whole evolution; at the beginning, our core finder measures the mass of a dominant core and afterwards what is seen is the mass of the core resulting from the multi-merger. Notice that the mass oscillates due to the time dependence of the average density (the gray lines of the plot at the left) and in average it has a growing trend. The last 2 Gyr of the values of  $M_c$  are used to calculate an average value and an uncertainty for each of the simulations.

used to calculate the core mass  $M_c$  with the recipe (9). Both, the spatially averaged density and  $M_c$  are time dependent. In black we show the average in time calculated with the whole formula (15). This plot illustrates how spatial averages change in time, more evidently in the envelope region.

Now, the time dependence of the spatial average (see the gray lines) implies a time-dependent value of  $M_c$ , which is

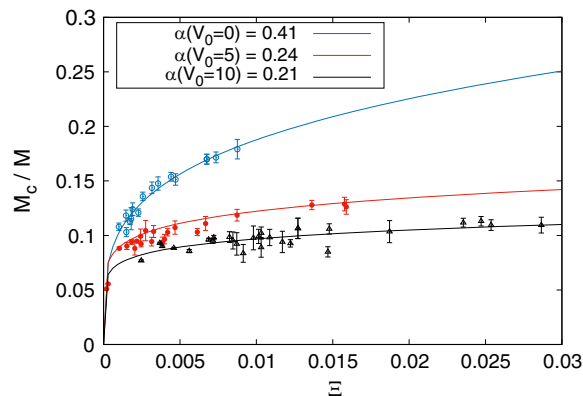


FIG. 3. We plot  $M_c/M$  vs  $\Xi$  for each of the simulations, and for the three cases with  $V_0 = 0, 5, 10$  in blue, red, and black respectively. Each point corresponds to the average of the values of  $M_c$  during the last 2 Gyr of each simulation, whereas the error bars are the standard deviation of the values used to calculate such average. The continuous lines are the best fitting lines using formula (10).

shown in the third plot of Fig. 2. This figure starts with the core mass of the dominant core among those in the initial set of random cores, its mass is calculated, and then, by  $t \sim 5$  Gyr, the final core starts to be formed. From then on,  $M_c$  oscillates around a growing value due to the accretion of matter from the envelope as found in [25]. We measure the values of  $M_c$  during the last 2 Gyr of evolution to calculate its time average and standard deviation that we use as experimental data and error bars respectively, in the study of the scaling relation below.

### C. Scaling relation

We simulate the multimergers and postprocess the data as described for a particular simulation above, until we obtain  $M_c$  as function of time like the results in Fig. 2. This value of  $M_c$  is calculated every 0.05 Gyr between 12 and 14 Gyr, we then calculate the average of the 41 values of  $M_c$  in such time window and the standard deviation of all these values is used to define an error bar in the value of  $M_c$ . This value, together with the integrals  $M$  and  $E$  in the whole domain define points in an  $M_c/M$  vs  $\Xi$  diagram. These points are then fitted with the ansatz (10) in order to find the best fitting values of  $\alpha$  and  $\beta$ .

The results are summarized in Fig. 3, where we show the fittings of the core-halo scaling relation with formula (10) obtained from our simulations using potentials  $V_A$  and the two cases  $V_B$ , specifically for  $V_0 = 0, 5, 10$ . The values of the exponent  $\alpha$  are respectively  $\alpha = 0.407 \pm 0.008$ ,  $0.237 \pm 0.011$ ,  $0.212 \pm 0.017$ .

For potential  $V_A$ , that is  $V_0 = 0$ , corresponding to the approximated monopolar boundary condition we find that the core-halo scaling relation has an exponent  $\alpha \approx 0.4$ , consistent with multicore mergers reported in [7] and the general structures constructed in cases of spherical symmetry [18] where the monopolar boundary condition is imposed by construction. On the other hand, for potential  $V_B$  with  $V_0 = 5, 10$ ,  $\alpha$  is close to  $\sim 1/4$ . Even though it is dynamically the same system, we show how by redefining the reference potential we find a different scaling relation.

## IV. CONCLUSIONS

We found that the core-halo scaling relation can vary, depending on the gravitational potential reference value. In periodic domains this may be the responsible for finding different values of  $\alpha$  out of different simulation scenarios and domain sizes. We illustrate this result using the  $V_0$ -gauge invariance on the particular scenario of multicore mergers. We speculate that the nonstandardization of the reference gravitational potential in the various simulations may be one of the reasons for the dispersion and diversity of the scaling relation studied in e.g. [9,19].

Notice that the result in this paper applies to the case in which the domain is periodic and a value of the potential is used in the faces of the domain. The potential shifting does not apply to the case in which isolated boundary conditions are used, as done in [13].

## ACKNOWLEDGMENTS

Iván Álvarez receives support within the CONACyT graduate scholarship program under the CVU 967478. This research is supported by grants CIC-UMSNH-4.9 and CONACyT Ciencias de Frontera Grant No. Sinergias/304001. The runs were carried out in the facilities of the Laboratorio Nacional de Cómputo de Alto Desempeño under Grant No. 1-2024.

[1] Abril Suárez, Victor H. Robles, and Tonatihu Matos, A review on the scalar field/Bose-Einstein condensate dark matter model, *Astrophys. Space Sci. Proc.* **38**, 107 (2014).

[2] Lam Hui, Wave dark matter, *Annu. Rev. Astron. Astrophys.* **59**, 247 (2021).

[3] Elisa G.M. Ferreira, Ultra-light dark matter, *Astron. Astrophys. Rev.* **29**, 7 (2021).

- [4] Pierre-Henri Chavanis, Self-gravitating Bose-Einstein condensates, in *Quantum Aspects of Black Holes*, edited by Xavier Calmet (Springer International Publishing, Cham, 2015), pp. 151–194.
- [5] Jens C. Niemeyer, Small-scale structure of fuzzy and axion-like dark matter, *Prog. Part. Nucl. Phys.* **113**, 103787 (2020).
- [6] Hsi-Yu Schive, Tzihong Chiueh, and Tom Broadhurst, Cosmic structure as the quantum interference of a coherent dark wave, *Nat. Phys.* **10**, 496 (2014).
- [7] Philip Mocz, Mark Vogelsberger, Victor H. Robles, Jesus Zavala, Michael Boylan-Kolchin, Anastasia Fialkov, and Lars Hernquist, Galaxy formation with BECDM I. Turbulence and relaxation of idealized haloes, *Mon. Not. R. Astron. Soc.* **471**, 4559 (2017).
- [8] Jan Veltmaat, Jens C. Niemeyer, and Bodo Schwabe, Formation and structure of ultralight bosonic dark matter halos, *Phys. Rev. D* **98**, 043509 (2018).
- [9] Simon May and Volker Springel, Structure formation in large-volume cosmological simulations of fuzzy dark matter: Impact of the non-linear dynamics, *Mon. Not. R. Astron. Soc.* **506**, 2603 (2021).
- [10] Bodo Schwabe and Jens C. Niemeyer, Deep zoom-in simulation of a fuzzy dark matter galactic halo, *Phys. Rev. Lett.* **128**, 181301 (2022).
- [11] W. Hu, R. Barkana, and A. Gruzinov, Fuzzy cold dark matter: The wave properties of ultralight particles, *Phys. Rev. Lett.* **85**, 1158 (2000).
- [12] Hsi-Yu Schive, Ming-Hsuan Liao, Tak-Pong Woo, Shing-Kwong Wong, Tzihong Chiueh, Tom Broadhurst, and W. Y. Pauchy Hwang, Understanding the core-halo relation of quantum wave dark matter from 3D simulations, *Phys. Rev. Lett.* **113**, 261302 (2014).
- [13] Bodo Schwabe, Jens C. Niemeyer, and Jan F. Engels, Simulations of solitonic core mergers in ultralight axion dark matter cosmologies, *Phys. Rev. D* **94**, 043513 (2016).
- [14] F. S. Guzmán and L. Arturo Ureña López, Evolution of the Schrödinger-Newton system for a self-gravitating scalar field, *Phys. Rev. D* **69**, 124033 (2004).
- [15] J. Luna Zagorac, Emily Kendall, Nikhil Padmanabhan, and Richard Easther, Soliton formation and the core-halo mass relation: An eigenstate perspective, *Phys. Rev. D* **107**, 083513 (2023).
- [16] Matteo Nori and Marco Baldi, Scaling relations of fuzzy dark matter haloes. I. Individual systems in their cosmological environment, *Mon. Not. R. Astron. Soc.* **501**, 1539 (2020).
- [17] Mattia Mina, David F. Mota, and Hans A. Winther, Solitons in the dark: First approach to non-linear structure formation with fuzzy dark matter, *Astron. Astrophys.* **662**, A29 (2022).
- [18] Iván Álvarez-Rios and Francisco S. Guzmán, Spherical solutions of the Schrödinger-Poisson system with core-tail structure, *Phys. Rev. D* **108**, 063519 (2023).
- [19] Hei Yin Jowett Chan, Elisa G M Ferreira, Simon May, Kohei Hayashi, and Masashi Chiba, The diversity of core-halo structure in the fuzzy dark matter model, *Mon. Not. R. Astron. Soc.* **511**, 943 (2022).
- [20] Xiaolong Du, Christoph Behrens, Jens C. Niemeyer, and Bodo Schwabe, Core-halo mass relation of ultralight axion dark matter from merger history, *Phys. Rev. D* **95**, 043519 (2017).
- [21] Iván Álvarez-Rios, Francisco S. Guzmán, and Paul R. Shapiro, Effect of boundary conditions on structure formation in fuzzy dark matter, *Phys. Rev. D* **107**, 123524 (2023).
- [22] Edward Seidel and Wai-Mo Suen, Formation of solitonic stars through gravitational cooling, *Phys. Rev. Lett.* **72**, 2516 (1994).
- [23] F. S. Guzmán and L. Arturo Ureña López, Gravitational cooling of self-gravitating Bose condensates, *Astrophys. J.* **645**, 814 (2006).
- [24] Iván Álvarez-Rios and Francisco S. Guzmán, Exploration of simple scenarios involving fuzzy dark matter cores and gas at local scales, *Mon. Not. R. Astron. Soc.* **518**, 3838 (2022).
- [25] Jiajun Chen, Xiaolong Du, Erik W. Lentz, David J.E. Marsh, and Jens C. Niemeyer, New insights into the formation and growth of boson stars in dark matter halos, *Phys. Rev. D* **104**, 083022 (2021).